Supporting Information

In Situ Synthesis of Vacancy-Rich Titanium Sulfide Confined in a Hollow Carbon Nanocage as an Efficient Sulfur Host for Lithium−Sulfur Batteries

Yiming Zhang[†], *Yubing Si*[†], *Wei Guo, Xiang Li, Shuai Tang, Zhaoxin Zhang, Xin Wang* and Yongzhu Fu**

College of Chemistry, Zhengzhou University, Zhengzhou 450001, P. R. China

*Corresponding authors: wangxin0620@zzu.edu.cn (X. Wang) and yfu@zzu.edu.cn (Y. Fu)

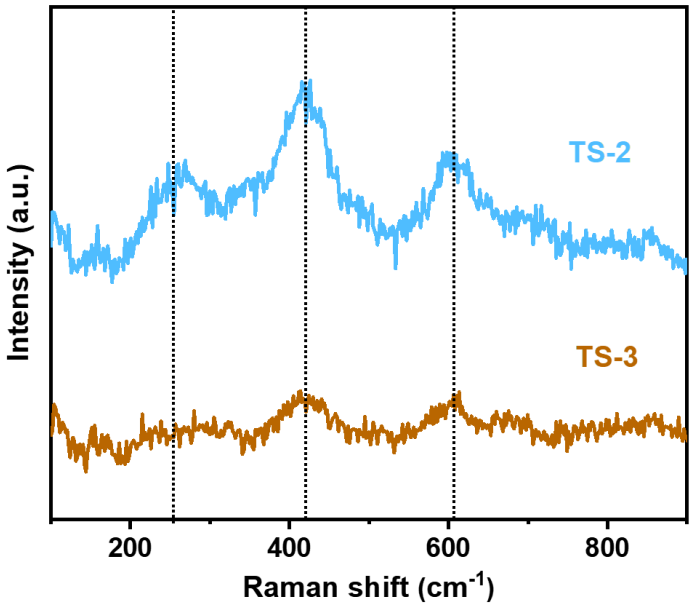

Figure S1. Raman spectra of TiS_x@HCN with the different ratios (1:2 & 1:3) of titanium and sulfur powder denoted as TS-2 and TS-3, respectively.

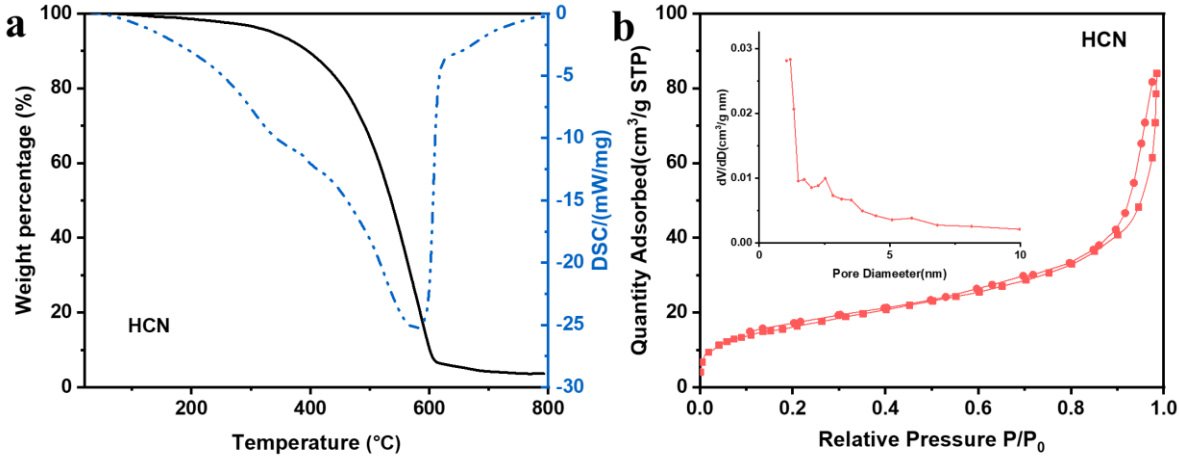

Figure S2. a) TG curve and DTA analysis of HCN; b) N_2 adsorption-desorption isotherms and pore size distributions (insert) of HCN.

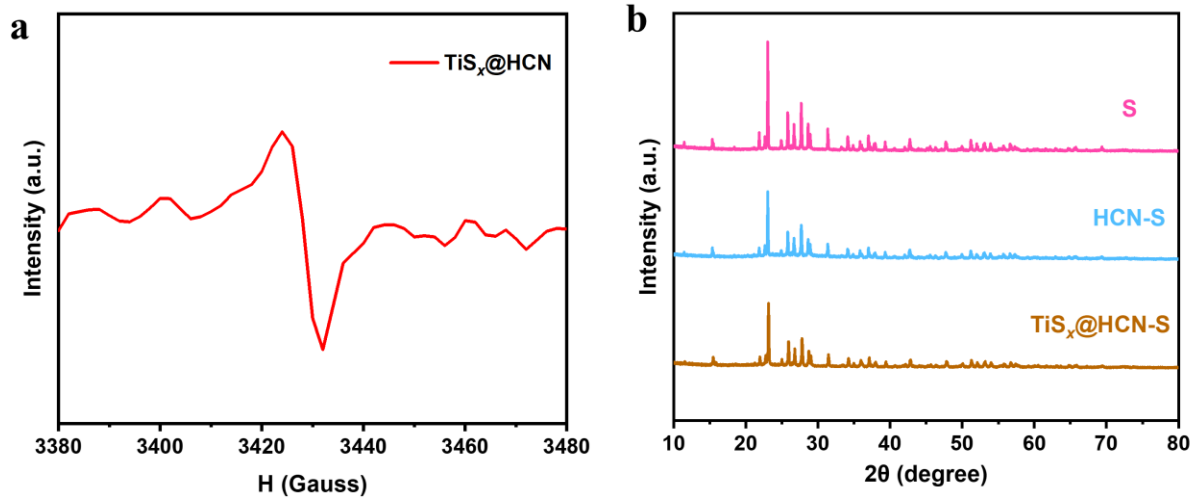

Figure S3. a) EPR spectra of TiS_x@HCN. b) XRD patterns of S, HCN-S, and TiS_x@HCN-S.

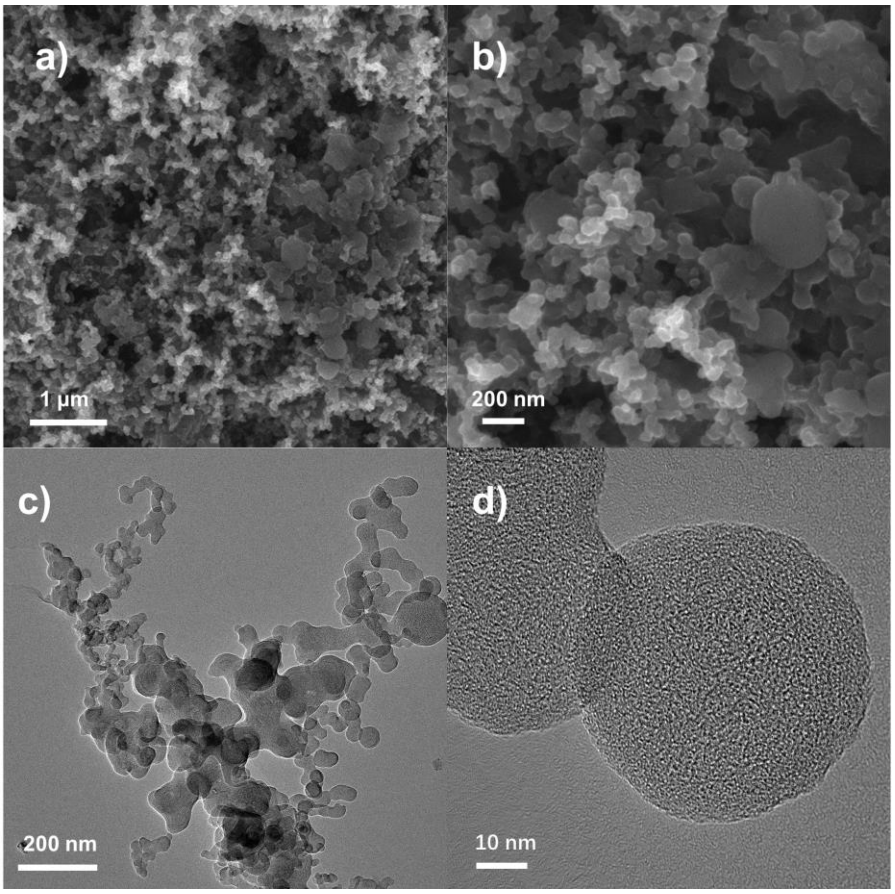

Figure S4. SEM images of (a & b) HCN and TEM images of (c & d) HCN.

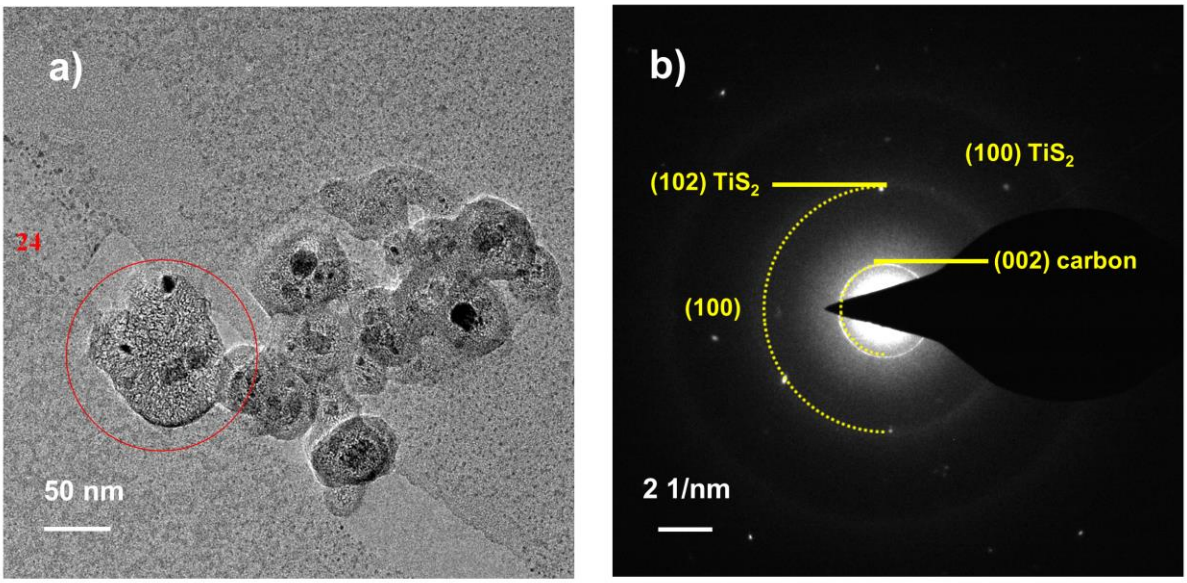

Figure S5. a) TEM image and b) SAED pattern of TiS_x@HCN.

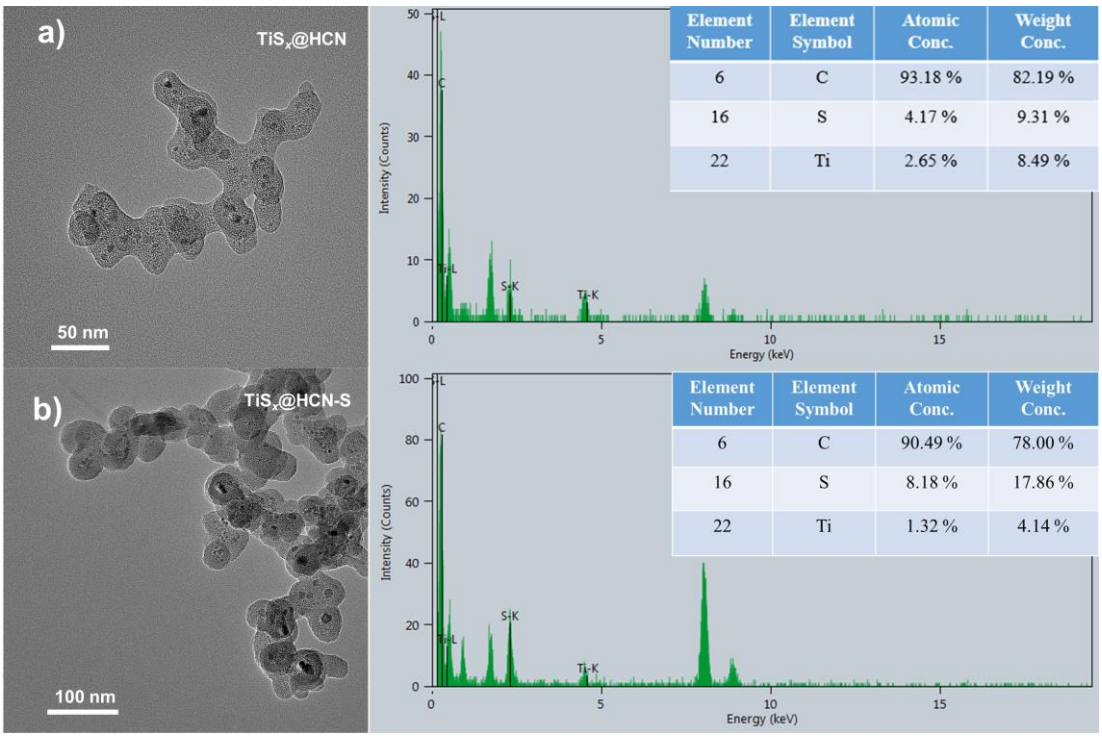

Element Number	Element Symbol	Atomic Conc.	Weight Conc.
6	C	93.18 %	82.19 %
16	S	4.17 %	9.31 %
22	Ti	2.65 %	8.49 %

Element Number	Element Symbol	Atomic Conc.	Weight Conc.
6	C	90.49 %	78.00 %
16	S	8.18 %	17.86 %
22	Ti	1.32 %	4.14 %

Figure S6. a) The low-magnification TEM image and EDX spectrum of amorphous TiS_x@HCN. The atomic ratio of Ti/S is about 2:3. b) The low-magnification TEM image and EDX spectrum of amorphous TiS_x@HCN-S. The atomic ratio of Ti/S is about 1:6.

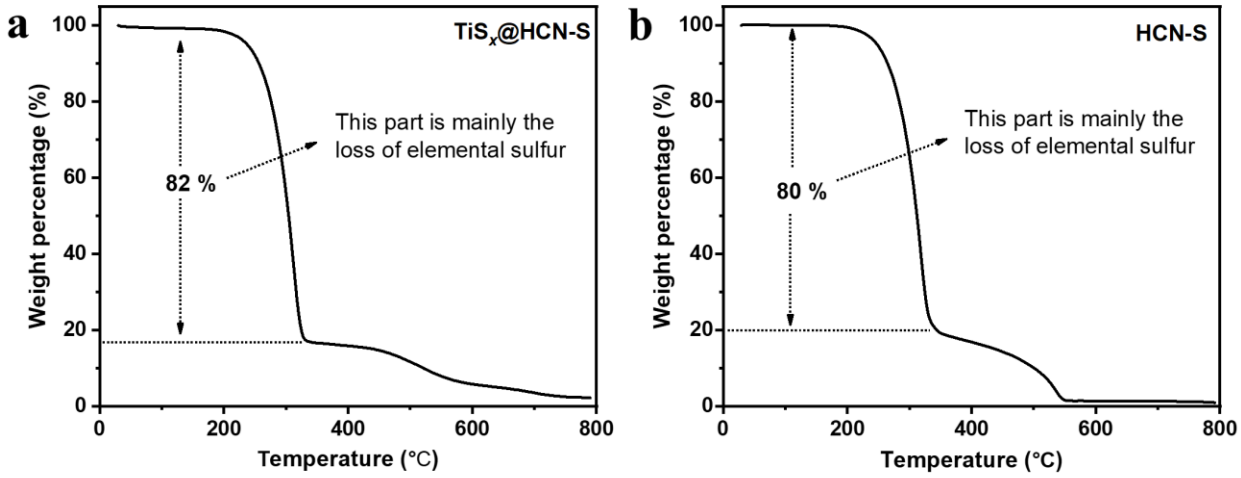

Figure S7. TGA curves of TiS_x@HCN-S (a) and HCN-S (b).

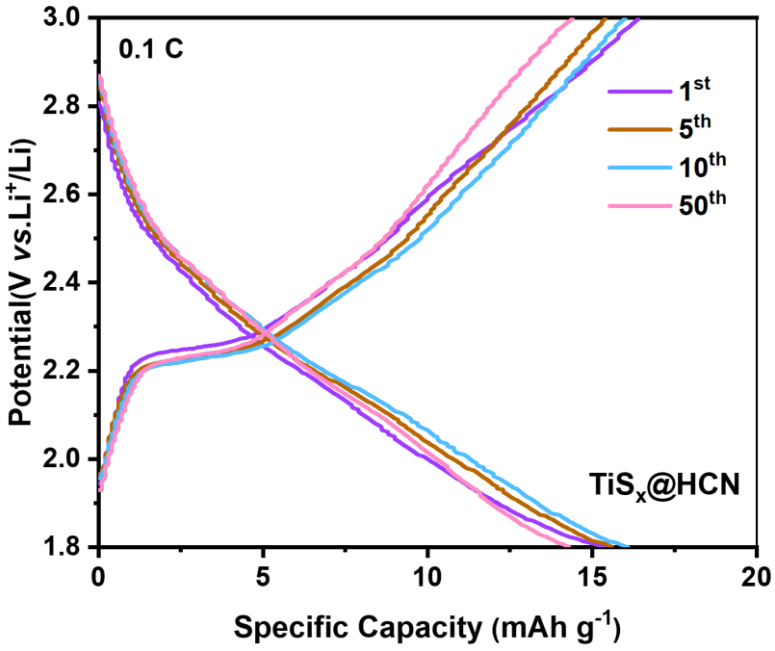

Figure S8. The galvanostatic charge-discharge voltage profiles of pure TiS_x@HCN cathode for the initial 50 cycles at the rate of 0.1 C. The specific capacity was measured corresponding to the mass of TiS_x. Note: It can be clearly seen that the pure TiS_x electrode has no obvious charge/discharge voltage plateaus and shows a negligible capacity less than 20 mAh g^{-1}, which has almost no contribution to the measured capacity of Li-S batteries.

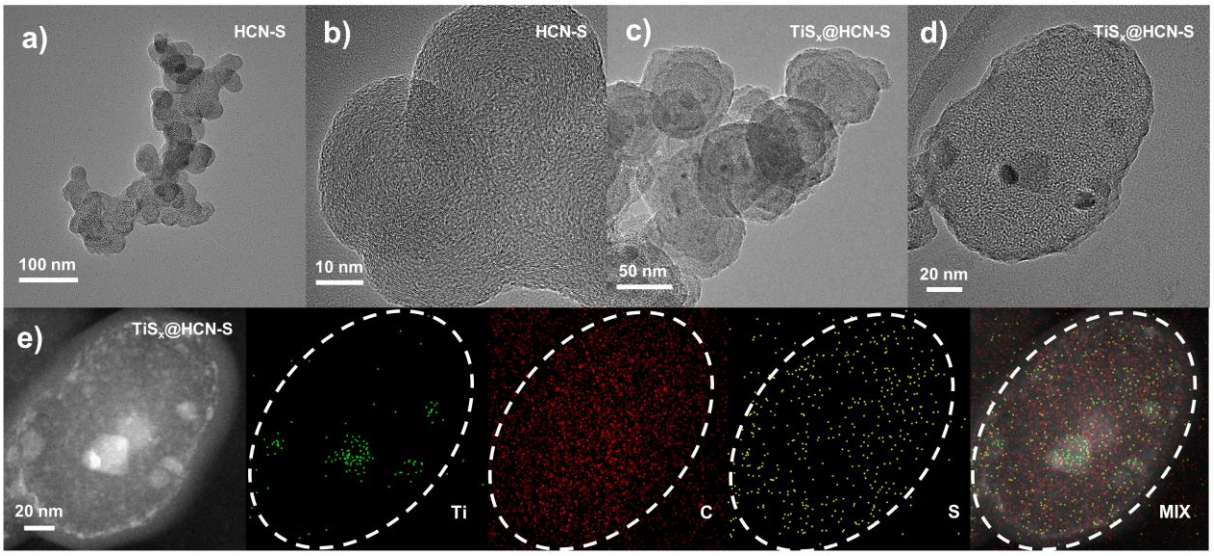

Figure S9. TEM images of HCN-S (a & b) and TiS_x@HCN-S (c & d) cathode after 400 cycles at 0.5 C. (e) Elemental mapping (C, Ti, & S) images of TiS_x@HCN-S cathode after 400 cycles.

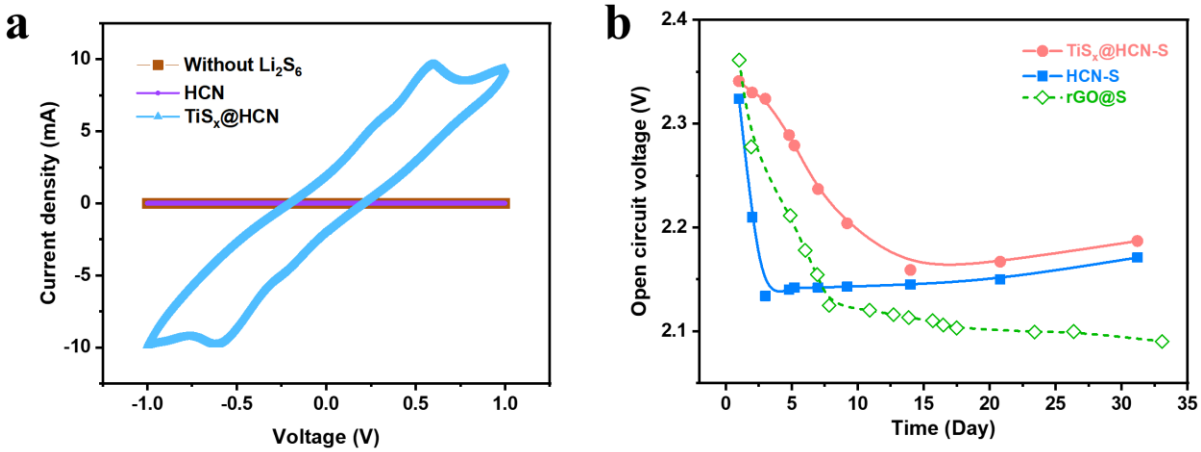

Figure S10. a) CV plots of the symmetric cells with HCN and TiS_x@HCN electrodes at a scan rate of 10 mV s^{-1}. b) Open-circuit voltages of the cells with TiS_x@HCN-S, HCN-S, and rGO@S[1] cathodes.

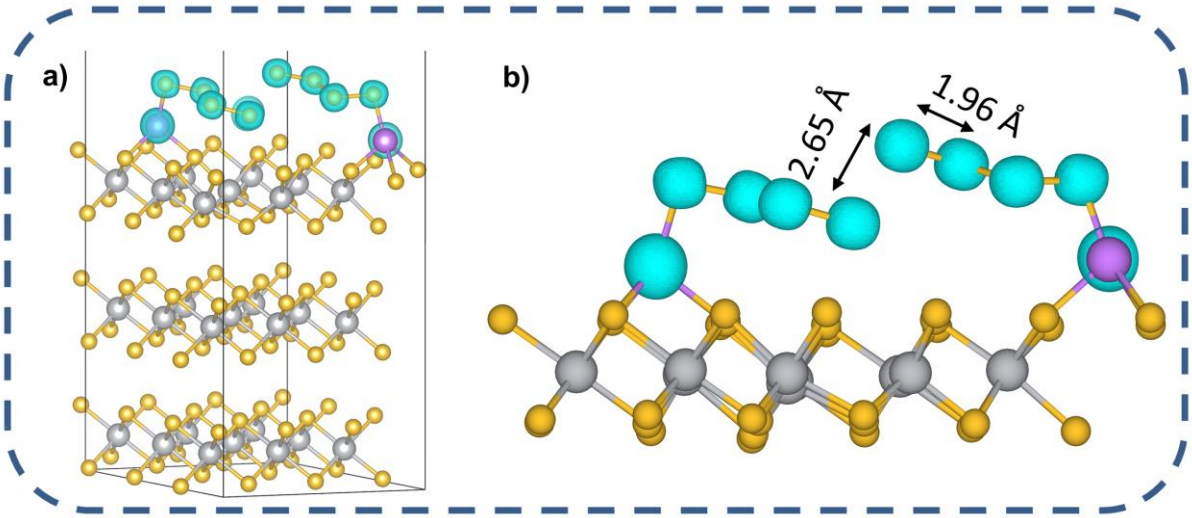

Figure S11. The scheme of Li_2S_8 adsorbed on the defected-TiS_2 surface. The elongated (2.65 Å) and normal S-S bond (1.96 Å) are labeled in Figure b.

Table S1. Elemental analysis results of TiS_x@HCN based on the SEM-EDS and TEM-EDS.

Method	Element	Atomic Concentration (at. %)	Atomic Error (%)	Weight Concentration (wt. %)	Mass Error (%)
SEM-EDS	Ti K	1.58	/	5.76	/
	S K	2.89	/	7.05	/
TEM-EDS	Ti K	2.65	0.85	9.31	1.89
	S K	4.17	0.41	8.49	1.30

Table S2. Elemental analysis results of TiS_x@HCN-S and HCN-S cathodes after 400 cycles at 0.5 C based on the TEM-EDS.

Cathode	Element	Atomic Concentration (at. %)	Atomic Error (%)	Weight Concentration (wt. %)	Mass Error (%)
TiS_x@HCN-S	S K	2.64	0.53	6.16	1.23
HCN-S	S K	0.26	0.14	0.66	0.30

Table S3. Comparison of the cycling stability of this work with other reported works with the similar structure.

Cathode materials	Initial capacity (mAh g^{-1})	Cycle number	Cycling rate	Capacity decay rate per cycle
This work	1118.6	200	0.1 C	0.108%
MoO_2/C-S[2]	734	400	0.5 C	0.1%
S-FeS@G/CNT[3]	705	300	0.5 C	0.175%
S/WO3[4]	769	100	0.2 C	0.56%
S/WC[4]	843	100	0.2 C	0.18%
S/MgO[5]	860	100	0.2 C	0.18%
FeS/C-S[6]	870	100	0.1 C	0.338%
TiS_{2-x}/S[7]	1169.8	100	0.2 C	0.21%
rGO/N-YSHCS/S[8]	1100.41	100	0.2 C	0.273%
S@SiO_2[9]	1153	100	0.2 C	0.292%

REFERENCES

1. Yu, P.; Feng, L.-X.; Ma, D.-C.; Sun, X.-R.; Pei, J.-K.; Zha, X.-J.; Bao, R.-Y.; Wang, Y.; Yang, M.-B.; Guo, Z.-P.; Yang, W. Template-Free Self-Caging Nanochemistry for Large-Scale Synthesis of Sulfonated-Graphene@Sulfur Nanocage for Long-Life Lithium-Sulfur Batteries. *Adv. Funct. Mater.* **2021**, *31*, 2008652.

2. Wang, C. L.; Sun, L. S.; Wang, X. X.; Wang, L. M. Spherical Hybrid Hierarchical Porous Structure: A Plastic Model with Tunable Inner Pores for Lithium-Sulfur Batteries. *Carbon* **2019**, *153*, 691-698.

3. Zhou, G. M.; Tian, H. Z.; Jin, Y.; Tao, X. Y.; Liu, B. F.; Zhang, R. F.; Seh, Z. W.; Zhuo, D.; Liu, Y. Y.; Sun, J.; Zhao, J.; Zu, C. X.; Wu, D. S.; Zhang, Q. F.; Cui, Y. Catalytic Oxidation of Li_2S on the Surface of Metal Sulfides for Li-S Batteries. *Proc. Natl. Acad. Sci. U. S. A.* **2017**, *114*, 840-845.

4. Choi, J.; Jeong, T. G.; Cho, B. W.; Jung, Y.; Oh, S. H.; Kim, Y. T. Tungsten Carbide as a Highly Efficient Catalyst for Polysulfide Fragmentations in Li-S Batteries. *J. Phys. Chem. C* **2018**, *122*, 7664-7669.

5. Ponraj, R.; Kannan, A. G.; Ahn, J. H.; Kim, D. W. Improvement of Cycling Performance of Lithium-Sulfur Batteries by Using Magnesium Oxide as a Functional Additive for Trapping Lithium Polysulfide. *ACS Appl. Mater. Interfaces* **2016**, *8*, 4000-4006.

6. Yuan, Q.; Chen, Y. X.; Li, A.; Li, Y. X.; Chen, X. H.; Jia, M. Q.; Song, H. H. Polysulfides Anchoring and Enhanced Electrochemical Kinetics of 3D Flower-Like FeS/Carbon Assembly Materials for Lithium-Sulfur Battery. *Appl. Surf. Sci.* **2020**, *508*, 145286.

7. Zhao, Y.; Cai, W.; Fang, Y.; Ao, H.; Zhu, Y.; Qian, Y. Sulfur-Deficient TiS_{2-x} for Promoted Polysulfide Redox Conversion in Lithium-Sulfur Batteries. *ChemElectroChem* **2019**, *6*, 2231-2237.

8. Zhang, Y. Z.; Sun, K.; Zhan, L.; Wang, Y. L.; Ling, L. C. N-Doped Yolk-Shell Hollow Carbon Sphere Wrapped with Graphene as Sulfur Host for High-Performance Lithium-Sulfur Batteries. *Appl. Surf. Sci.* **2018**, *427*, 823-829.

9. Liu, T. T.; Zhang, Y.; Li, C. H.; Marquez, M. D.; Tran, H. V.; Hernandez, F. C. R.; Yao, Y.; Lee, T. R. Semihollow Core-Shell Nanoparticles with Porous SiO_2 Shells Encapsulating Elemental Sulfur for Lithium-Sulfur Batteries. *ACS Appl. Mater. Interfaces* **2020**, *12*, 47368-47376.